Sustainable Cities and Society 137 (2026) 107129

Contents lists available at ScienceDirect

Sustainable Cities and Society

journal homepage: www.elsevier.com/locate/scs

Rooftop PV layout generation and optimization model for large-scale building cluster

Rui Miao [a], Haoqing Zhu [b], Yi Zhang [a,*], Kanghua Li [a], Yuan Yuan [a], Pengyuan Shen [a], He Qi [c]

[a] Institute of Future Human Habitats, Tsinghua Shenzhen International Graduate School, Tsinghua University, Shenzhen 518055, China
[b] Hangzhou Yuhang District Bureau of Housing and Urban-Rural Development, Hangzhou, China
[c] China Construction Science and Technology Group, 2007 Pingshan Avenue, Shenzhen 518118, China

ARTICLE INFO

Keywords:
Rooftop PV
Large-scale PV planning
Rooftop availability
Multi-objective optimization
Computational efficiency

ABSTRACT

Rooftop photovoltaic (PV) deployment at the cluster scale is critical for advancing urban decarbonization, yet existing methods often oversimplify available area estimation, neglect engineering constraints, and struggle to balance energy, economic, and environmental objectives. To address these gaps, this study proposes an integrated model comprising three modules: (1) high-fidelity identification of available rooftop area by explicitly excluding shadow area, obstacles with buffer zones, and maintenance pathways; (2) automated generation of 3D engineering-feasible PV layouts; and (3) a hybrid single- and multi-objective optimization with TOPSIS-based decision-making. Applied to a 245-building cluster in Shenzhen, the model identified 23,982 m^2 of available area (46.51 % ratio), more conservative than typical utilization-factor assumptions. It generated detailed 3D, module-level PV layouts for 198 buildings, enabling high-fidelity PV output simulation accounting for site-specific orientation, tilt, and shading. Across all budget levels, the optimized solutions outperformed 30,000 random alternatives, with internal rates of return ranging from 16.1 % to 19.2 %. Under the high-budget scenario, the CEB-optimal solution, which utilizes all technically feasible rooftops, achieves a 10-year cumulative energy yield of 61.61 GWh and carbon emission reductions of 27,725.59 t CO_2. By decoupling layout generation from optimization, the framework reduces computational complexity and enables efficient generation of optimized deployment solutions. The proposed framework facilitates large-scale rooftop PV deployment and contributes to the decarbonization of urban energy systems.

1. Introduction

In the context of global climate change, achieving carbon neutrality has become a central objective for many nations (UNFCCC, 2015). Among various renewable energy technologies, solar photovoltaic (PV) systems have become one of the most widely adopted solutions because of their zero operational emissions, scalability, and abundant resource availability (Zhang et al., 2023). By the end of 2024, worldwide renewable energy capacity reached approximately 4,448 GW (Nassar et al., 2025), with over 600 GW of new solar PV capacity added, of which rooftop and distributed systems grew by 200 GW (REN21, 2025). In China, centralized large-scale photovoltaic (LSPV) systems are predominantly deployed in sparsely populated western regions (Sun et al., 2017), which offer vast suitable areas and an estimated potential of approximately 42.8 TW (Yu et al., 2023). However, delivering electricity from remote generation sites to eastern demand centers requires long-distance transmission, which incurs transmission losses of approximately 7 %, far exceeding the 2.5 % loss rate typical of distributed solar photovoltaic (DSPV) (Sun et al., 2017). To address these challenges, China has set an ambitious target of deploying 800 GW of rooftop PV capacity by 2035 (LBNL, 2025), reflecting a strategic shift toward DSPV and contributing to its carbon neutrality goals.

Research on rooftop PV deployment spans multiple scales. At the urban scale, studies primarily focus on assessing the rooftop PV potential across entire cities and translating these assessments into practical planning guidance. Wei et al. (2024) developed a city-scale PV deployment decision-making model for Shenzhen, clarifying deployment priorities and quantifying the electricity demand coverage ratio of different PV installation targets. Chen et al. (2022) proposed a cost-effective assessment method for Shanghai's downtown area,

* Corresponding author.
E-mail address: zy1214@sz.tsinghua.edu.cn (Y. Zhang).

https://doi.org/10.1016/j.scs.2026.107129
Received 25 February 2025; Received in revised form 24 December 2025; Accepted 5 January 2026
Available online 6 January 2026

achieving highly accurate solar radiation estimation and rooftop classification while quantifying PV systems' economic and ecological benefits. Cuesta-Fernández et al. (2023) proposed an urban-metropolitan energy exchange model, showing that expanding rooftop PV in Valencia's metropolitan area could significantly increase its PV coverage rate and support carbon neutrality goals. Building-scale studies focus on detailed optimization, including PV module layout efficiency and additional functionalities such as shading effects and thermal insulation (Nassar et al., 2019). For instance, to enhance indoor comfort when bifacial PV serves as building envelope, Zhao et al. (2022) improved annual thermal comfort period by 8 % via optimizing PV coverage and adding heat insulation layers. Focusing on the dual functionality of building-integrated PV (BIPV) in shading and power generation, Paydar (2020) developed a movable BIPV shading system, which achieved lower building annual thermal load and significantly higher excess electricity generation compared to multiple fixed modes.

To bridge the gap between city-wide potential estimates and single-building design, recent research has increasingly turned to the building cluster scale. Zhang et al. (2023) developed a multi-scale energy storage allocation model and demonstrated that cluster-level coordination of PV and storage can reduce annual energy costs by more than 55 %. Yu et al. (2023) proposed a classification-based framework for building clusters, enabling efficient estimation of PV potential across thousands of urban buildings. Ma et al. (2016) introduced the concept of smart building clusters and showed that coordinated PV and demand response strategies can reduce total operational costs by 4.6 % and improve load factors. Together, these works highlight the building cluster as a strategically valuable scale: it balances computational feasibility with engineering realism, offering a practical pathway for scaling up distributed PV deployment.

Research on PV deployment at the building cluster scale has largely focused on two key objectives: the estimation of available rooftop area and the generation of PV deployment plans. Yang et al. (2024) used a semi-supervised segmentation approach, Tian and Ooka (2025) applied parametric modeling with machine learning techniques, and Yan et al. (2023) adopted a detail-oriented deep learning method to estimate available rooftop area. However, all these approaches effectively rely on utilization factors, which are empirical coefficients that convert total roof area into assumed available area. They treat rooftops as uniformly installable and neglect fine-grained physical constraints such as shadow area, obstructions, and maintenance pathways, which are essential for accurately determining the actual available area for module-level PV installation (Nassar et al., 2022a, 2022b). Regarding the generation of PV deployment plans, Kucuksari et al. (2014) used LiDAR data and applied criteria related to irradiance, height, orientation, and slope to select installation sites. Santos et al. (2014) used only solar irradiance and rooftop area thresholds to filter candidates. Lee et al. (2018) introduced a bi-criteria rating system that classifies buildings along a suitability spectrum based on technical and economic factors. Ren et al. (2023) formulated the layout problem as a nonlinear integer program to maximize system capacity at the cluster scale. However, their planning frameworks treat rooftops as abstract two-dimensional surfaces defined by aggregated metrics, without representing physical constraints or generating module-level layouts. As a result, while effective for strategic prioritization, their outputs are not directly translatable into constructible PV designs. In contrast, recent studies have shifted toward generating physically realizable PV layouts by explicitly incorporating engineering and geometric constraints into the design process. Barbón et al. (2022) considered irregular rooftop geometries and module dimensions in an automated layout-generation algorithm, while Kontar and Jin (2020) integrated energy simulation, environmental analysis, and parametric modeling within a Grasshopper-based workflow to generate PV layouts. Despite their high fidelity, these approaches are typically implemented within 3D modeling environments, which are well suited for individual buildings or small clusters but encounter computational bottlenecks when applied to large-scale building clusters (Ren et al., 2023).

Existing studies on rooftop PV assessment have evolved from energy-focused evaluations toward more comprehensive approaches incorporating economic and environmental dimensions. Tao et al. (2025) evaluated rooftop PV performance using energy-based indicators such as the self-consumption rate (SCR) and self-sufficiency rate (SSR). Pan et al. (2022) analyzed the economic feasibility of urban rooftop PV deployment under multiple installation scenarios, highlighting the influence of system configuration on payback period and financial returns at the city scale. Šimić et al. (2021) proposed a PV sizing and decision-making model driven by economic performance, identifying optimal system sizes under regulatory and market constraints. Furthermore, Zhu et al. (2022), Li et al. (2023), and Allouhi (2020) adopted multi-dimensional evaluation frameworks that integrate economic and environmental considerations, introducing comprehensive indicators such as the levelized cost of energy (LCOE) and carbon emission metrics to capture the broader sustainability implications of rooftop PV deployment. This shift reflects growing awareness that rooftop PV deployment involves multiple, sometimes competing objectives, necessitating multidimensional evaluation for decision-making. Multi-objective optimization (MOO) has been increasingly adopted in urban photovoltaic research. Wang et al. (2025) developed a MOO framework for high-density urban blocks to optimize trade-offs among energy demand, solar access, and available surface area. Gao et al. (2025) proposed a techno-economic-environmental MOO framework for industrial rooftop PV energy-storage systems. Liu et al. (2023) applied a MOO approach to optimize PV–energy storage configurations in urban industrial buildings, identifying trade-offs among technical, economic, and environmental objectives. These studies illustrate the effectiveness of MOO in generating Pareto-optimal solutions to guide large-scale rooftop PV deployment. Among various algorithms, NSGA-II (Deb et al., 2002) has been widely adopted in studies on solar energy potential and building performance optimization, demonstrating its effectiveness in balancing multiple competing objectives.

Although previous studies have laid a solid foundation for the generation and optimization of rooftop PV deployment and for evaluating its multidimensional performance, few have developed an integrated framework that simultaneously ensures physical feasibility, computational scalability, and balanced multi-objective optimization for large-scale building clusters. Existing large-scale planning approaches often incorporate multiple performance criteria but typically represent rooftops as homogeneous planar surfaces, ignoring module-level installation constraints such as shadow area, obstructions, and maintenance pathways. As a result, they yield only aggregated capacity estimates rather than constructible layouts. In contrast, high-fidelity methods that embed detailed 3D geometry and engineering rules can generate physically realizable PV configurations, yet their high computational cost limits applicability to large-scale building clusters. To bridge this gap, this study proposes a novel model that unifies fine-grained physical realism with efficient multi-objective optimization, enabling the scalable generation of feasible, high-resolution PV layouts for building clusters. The main contributions of this research include:

1. A three-module framework for systematic PV layout generation and optimization, comprising: (i) an available rooftop area identification module that classifies shadow areas, roof obstacles with buffer zones, and maintenance access pathways; (ii) an initial layout generation module that maximizes PV deployment under engineering constraints; and (iii) an optimization and decision-making module employing a hybrid single- and multi-objective framework to balance energy, environmental, and economic performance under varying budget constraints.
2. Decoupled integration of high-fidelity layout generation and scalable optimization. The framework explicitly separates the physically constrained 3D layout generation from system-level performance optimization. The model first embeds installation-related parameters

directly into the layout generation phase within a 3D modeling environment, ensuring that the initial PV layouts are physically feasible. The subsequent optimization process then operates on this set of constructible initial solutions rather than searching the full high-dimensional layout space, significantly reducing computational complexity while preserving engineering realism.

3. A case study was conducted in a diverse building cluster in Shenzhen, spanning nearly 150,000 square meters and comprising over 245

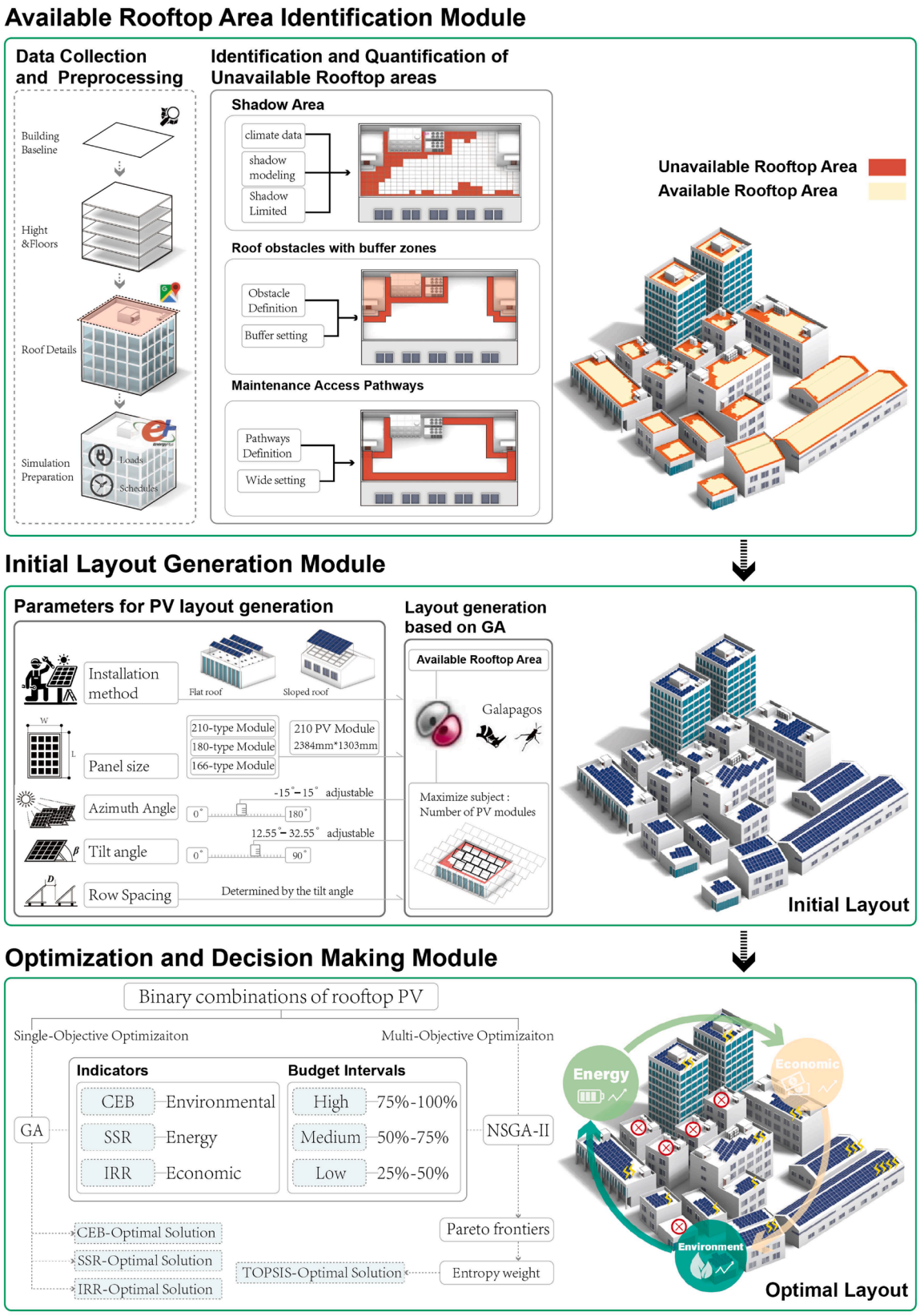

Fig. 1. Framework of the study.

buildings of various types. The results demonstrated the model's applicability and superior performance in complex building cluster environments.

The structure of this paper is as follows: Section 2 introduces the proposed PV layout generation and optimization model, detailing the methodology for identifying available rooftop areas, generating initial PV layouts, and conducting optimization. Section 3 presents the results of a case study conducted in a large-scale building cluster in Shenzhen, analyzing the performance of each module. Section 4 provides a comprehensive discussion of the implications, limitations, and scalability of the proposed approach. Finally, conclusions are presented in Section 5.

2. Methodology

Fig. 1 illustrates the overall framework of this study. First, the available rooftop area identification module prepares the building cluster dataset through data collection and preprocessing, then identifies unavailable areas to determine the available rooftop area for PV installation. After that, the initial layout generation module uses a genetic algorithm to produce a layout that maximizes PV deployment within the available areas while considering engineering constraints. Finally, the optimization and decision-making module integrates single-objective and multi-objective optimization frameworks under varying budget constraints to balance energy, environmental, and economic performance. The technical details and implementation of each module are described in the following sections.

2.1. Available rooftop area identification module

2.1.1. Data collection and preprocessing

Building outlines, heights, and floor counts were obtained from OpenStreetMap (OpenStreetMap, 2024) to generate 3D building models with Grasshopper (McNeel, 2024). High-resolution satellite imagery from Google Maps (Google, 2024) was combined with Rhinoceros (Rhinoceros, 2025) to model rooftop features, distinguishing sloped and flat roofs, which provide essential input for PV deployment planning. Building simulation settings, including material specifications, indoor activity schedules, and internal loads, were determined based on building function and Shenzhen's climate zone (ASHRAE 90.1-2013) (Deng et al., 2022). PV generation and energy consumption were simulated using ClimateStudio (Solemma, 2025), a Rhinoceros plugin powered by EnergyPlus (EnergyPlus, 2024). Local climate conditions were captured using a satellite-derived Typical Meteorological Year (TMYx) dataset (Ladybug Tools, 2025), ensuring realistic modeling of energy performance.

2.1.2. Identification and quantification of unavailable rooftop areas

In rooftop PV potential assessments, utilization-factor-based estimation remains widely used, but its accuracy is often limited in complex building environments. To improve upon this approach, Odeh and Nguyen (2021) introduced a roof suitability factor that integrates obstacle exclusion and roof tilt/orientation considerations, while Wang et al. (2022) proposed a method tailored to older residential buildings by removing areas occupied by rooftop structures and non-sunlit sloped surfaces. Building on these insights and incorporating practical installation guidelines from engineering standards, this study further refines rooftop availability estimation by classifying unavailable areas into three categories to support more accurate and safe PV deployment.

1) Shadow area:

Shadow significantly reduces the performance of PV modules and can even cause long-term damage (Ma et al., 2023). According to the Chinese National Standard GB50797-2012 (Ministry of Housing and Urban-Rural Development of the People's Republic of China, 2024), rooftop areas receiving less than 3 hours of sunlight during the winter solstice are classified as unavailable. Solar radiation simulations were conducted using the Ladybug plugin (Ladybug Tools, 2024) on the Grasshopper platform to accurately identify these shadowed areas.

2) Roof obstacles with buffer zones:

Certain rooftop structures and equipment are unsuitable for PV installation. For example, structures such as staircases and elevator shafts are typically excluded due to insufficient load-bearing capacity or installation difficulties. Additionally, rooftop equipment, such as water tanks and cooling towers, is also classified as unavailable (Cao et al., 2024). To ensure safe installation and maintenance, a 1.5-meter buffer zone was designated around these roof obstacles (Ma et al., 2023).

3) Maintenance Access Pathways:

Rooftop PV systems require designated pathways with a minimum width of 1.5 meters for maintenance personnel access (Ministry of Housing and Urban-Rural Development of the People's Republic of China, 2024). Therefore, a 1.5-meter-wide margin is reserved between the PV deployment area and the roof boundaries in this study.

By categorizing unavailable rooftop areas and integrating this information with the 3D building models from Section 2.1.1, this module identifies available rooftop areas. The identification results provide essential constraints for module placement, ensuring compliance with physical and regulatory requirements, which form a critical input for the initial layout generation in Section 2.2.

2.2. Initial layout generation module

2.2.1. Parameters for PV layout generation

1) Installation methods

In practical engineering applications, PV modules must be installed using methods selected according to the structural characteristics of the roof (Bahaj, 2003). This study selected commonly used and efficient installation methods for flat and sloped roofs, as illustrated in Fig. 2. For flat roofs, a concrete foundation installation method was adopted, which permits adjustments to the azimuth angle and row spacing by repositioning the concrete bases, while the tilt angle is controlled by varying the lengths of the metal supports (Bayod-Rújula et al., 2011). For sloped roofs, a clamp-based installation method was adopted, with PV modules mounted parallel to the roof slope and arranged edge-to-edge (Stenabaugh et al., 2015).

2) PV module dimensions

Among various PV module types such as 166, 180, and 210 (EE Power, 2024), the 210-type has become the dominant choice in China, accounting for over 60 % of production due to its high efficiency and mature supply chain (BJX, 2025). Given its widespread adoption, standardized dimensions (2382 mm × 1134 mm; see Fig. 3), and suitability

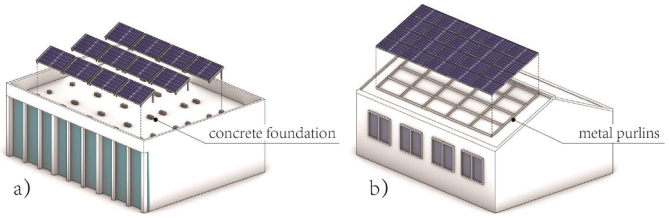

Fig. 2. PV installation methods. a) flat roofs. b) sloped roofs.

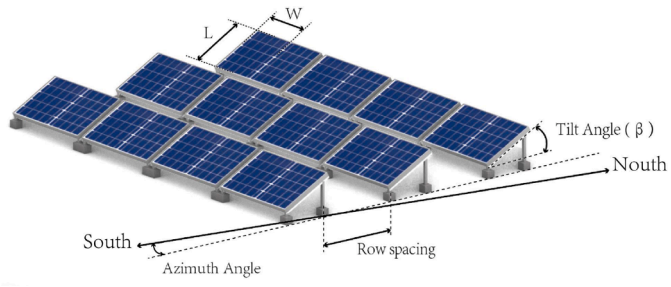

Fig. 3. Parameters for rooftop PV installation.

for large-scale applications, this study adopts the 210-type module as the reference specification.

3) Azimuth angle

Azimuth angle refers to the angle between the true south direction and the direction in which the PV module's vertical plane faces, measured in the horizontal plane. In the Northern Hemisphere, when the module's vertical plane faces true south, the azimuth angle is 0°, resulting in the maximum annual energy output from the module (Hafez et al., 2017). The azimuth angle can be adjusted by repositioning the concrete bases. In this study, the azimuth angle was allowed to vary within a ±15° range, where such variation has an acceptable impact on the efficiency of individual modules (Hafez et al., 2017; Meng et al., 2020; Chen et al., 2020).

4) Tilt angle

The tilt angle is the angle between the plane of the PV module and the horizontal ground. In rooftop PV projects, the optimal tilt angle is typically related to the local geographic latitude, with higher latitudes requiring a larger optimal tilt angle (Nassar et al., 2025). In regions with snowfall during winter, the tilt angle should also account for the snow shedding angle, but this factor is not considered in low-latitude regions (Jelle, 2013). Given Shenzhen's latitude (22.55°), the tilt angle was set within the range of 22.55°±10° to balance annual energy output and module spacing constraints.

5) Row spacing

Row spacing refers to the distance between PV modules in the north-south direction. This parameter plays a vital role in both energy efficiency and the safe operation of the rooftop PV system. As shown in Equation (1), row spacing can be calculated using the length of the PV module's long side, the tilt angle, and the latitude of the project location.

$$RowSpacing = L\sin\beta \cdot \frac{0.707\tan\phi + 0.4338}{0.707 - 0.4338\tan\phi} \quad (1)$$

where L is the length of the long side of PV module; β is the tilt angle of PV module (see Fig. 3);ϕ is the latitude of the PV project location. Therefore, adjusting the tilt angle can optimize the number of modules in the PV system by changing the row spacing of PV, thereby increasing the overall energy output of the system.

2.2.2. Initial layout generation

This study utilized the genetic algorithm plugin Galapagos (Rutten, 2024) on the parametric 3D modeling platform Grasshopper to generate an initial layout. The optimization objective was to maximize the number of deployable PV modules. The key parameters used in the optimization are summarized in Table 1, and the overall optimization workflow is illustrated in Fig. 4.

For flat roofs, a north-south oriented bounding rectangle was constructed based on the roof geometry and expanded by 10 % to ensure full coverage during the optimization process. This expansion ratio was confirmed through sensitivity testing (Section 3.5). Within the bounding rectangle, square PV units of 2382 mm × 2382 mm were generated, each integrating two 210-type modules placed side by side along their longer edges, with the extra width accounting for installation clearance. The initial configuration for each PV unit was set with an azimuth angle of 0°, a tilt angle of 22.55°, and the corresponding row spacing. To determine the optimal PV module configuration within available rooftop areas, a genetic algorithm was employed to search over three decision variables: rotation angle, tilt angle, and X/Y offset, within predefined ranges. These ranges and corresponding mutation steps were determined based on practical engineering constraints, energy performance considerations, and sensitivity analyses (Section 3.5), as summarized in Table 1. To improve computational efficiency, the optimization problem was transformed into a 2D planar problem, with PV unit projections screened to ensure they were fully contained within available areas defined in Section 2.1. For sloped roofs, the tilt angle is fixed due to the installation method; all other layout steps, including bounding rectangle construction and positional sampling, follow the same procedure as for flat roofs.

Table 1
Algorithm parameters and constraints of the optimization framework.

Category	Parameter	Value
Algorithm framework	Crossover probability	0.6
	Mutation probability	0.3
	Population size	150
	Number of generations	50
Decision variable ranges	Rotation angle range	[-15, 15] ° (mutation step: 1°)
	Tilt angle range	[12.55, 32.55] ° (mutation step: 1°)
	Offset range (X/Y direction)	[-5,5] (mutation step: 0.2 m)
Selection & operator	Selection strategy	Tournament selection (tournsize=2)
	Crossover operator	Blend crossover (α=0.5)
Fitness evaluation	Fitness function	Number of valid PV panels

2.3. Optimization and decision-making module

Building upon the initial layout in Section 2.2, a hybrid optimization framework combining single- and multi-objective approaches is implemented to balance environmental, energy, and economic performance under varying budget constraints. For each building, a binary decision variable (0 or 1) indicates whether its initial PV layout is retained. The optimization is performed across three budget scenarios representing high, medium, and low resource availability levels. During evaluation, only buildings with PV deployment (binary = 1) are included in cluster-level performance calculations, while non-PV buildings are excluded.

For single-objective optimization, the Genetic Algorithm (Holland, 1992) is employed to maximize individual performance metrics under each budget interval, generating targeted solutions to meet the demand for prioritizing a single performance dimension. For multi-objective optimization, the NSGA-II genetic algorithm is utilized to generate a Pareto front of non-dominated solutions (Verma et al., 2021), with parallel computing accelerating its computation (Chapman et al., 2007). However, for practical implementation, a single actionable layout is often required. To provide a transparent and interpretable selection from the Pareto front generated by NSGA-II, the TOPSIS (Hwang and Yoon, 1981) method is employed. TOPSIS has been extensively used in multi-objective optimization problems due to its conceptual simplicity and effectiveness in identifying balanced compromise solutions (Wang et al., 2025). To ensure objective and unbiased weight assignment, the Entropy method is adopted to determine the weights of the energy,

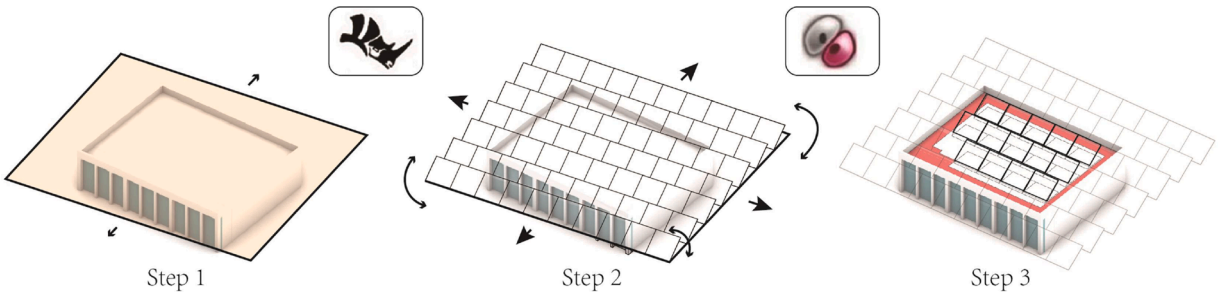

Fig. 4. Layout generation steps illustration.

environmental, and economic indicators based on their information entropy: indicators with lower entropy (i.e., higher data dispersion and stronger discriminatory power) are assigned higher weights (Arce et al., 2015). TOPSIS then ranks solutions according to their relative closeness to the ideal and anti-ideal points, with the top-ranked solution selected as the optimal actionable layout (Arce et al., 2015).

2.3.1. Performance indicators

1) Environmental performance:

Carbon emissions provide critical insight into the decarbonization potential of distributed renewable energy systems (Nassar et al., 2025). Carbon Emission Benefits (CEB), measured in kg CO_2, are used to evaluate the environmental performance of the project by quantifying the total carbon emissions reduced through PV deployment (Breyer et al., 2015). In this work, CEB is calculated over a 10-year operational period and accounts for PV module degradation to reflect realistic long-term environmental impacts. The calculation equations are as follows:

$$\mathrm{CEB} = G_{\mathrm{total}} \cdot f_{\mathrm{carbon}} \tag{2}$$

$$G_{\mathrm{total}} = \sum_{i=1}^{N} \sum_{t=1}^{T} G_{i,t} \tag{3}$$

$$G_{i,t} = G_{i,t,0} \cdot (1 - r_{\mathrm{PV}})^{y} \tag{4}$$

where G_{total} is the total PV generation of the building cluster, in kWh; f_{carbon} is the emission factor of the China Southern Power Grid, which is 0.45 kg CO_2/kWh (Ministry of Ecology and Environment of China MEE, 2025); $G_{i,t}$ is the PV generation of building i at time t, in kWh; $G_{i,t,0}$ is the first-year hourly PV generation for each building which can be obtained through simulation; r_{PV} is the annual degradation rate of PV panels, which is 0.004 (Longi, 2025).

2) Energy performance:

Self-sufficiency rate (SSR) is a key metric for evaluating the energy performance of PV systems (Tao et al., 2025). In this study, electricity generated by the rooftop PV system is primarily consumed within the same building, with any excess generation fed back into the grid (Zhang et al., 2023), as shown in Equation (5). SSR represents the proportion of a building's total energy demand that is supplied by its PV system, highlighting the extent to which the building reduces its reliance on the grid.

$$\mathrm{SSR} = \frac{\sum_{i=1}^{N} \sum_{t=1}^{T} E_{i,t}^{\mathrm{self}}}{\sum_{i=1}^{N} \sum_{t=1}^{T} E_{i,t}} \tag{5}$$

where $E_{i,t}^{\mathrm{self}}$ is the PV generation consumed by building i at time t, calculated as shown in Equation (6); $E_{i,t}$ is the energy consumption of building i at time t, calculated as shown in Equation (7).

$$E_{i,t}^{\mathrm{self}} = \min\left(E_{i,t}, G_{i,t}\right) \tag{6}$$

$$E_{i,t} = E_{i,t,0} \cdot \left(1 + r_{\mathrm{Energy}}\right)^{y} \tag{7}$$

$E_{i,t,0}$ is the first-year hourly energy consumption for each building, which can be obtained through simulation; r_{Energy} is the annual growth rate of building energy consumption, which is 0.05.

3) Economic performance:

The Internal Rate of Return (IRR) (Talavera et al., 2010) is used to evaluate the economic performance of the PV project for the building cluster. This study incorporates detailed costs of the PV project and distinguishes between commercial, industrial, and residential electricity tariffs, as shown in Equations (8), (9) and (10):

$$0 = \sum_{t=1}^{T} \frac{F_{\mathrm{cash},y}}{(1 + \mathrm{IRR})^{y}} - \mathrm{TotalInitialInvestment} \tag{8}$$

$$\mathrm{TotalInitialInvestment} = \sum_{i=1}^{N} \mathrm{InitialInvestment}_{i} \tag{9}$$

$$\mathrm{InitialInvestment}_{i} = P_i \cdot C_{\mathrm{PV}} \tag{10}$$

where $F_{\mathrm{cash},y}$ is the cash flow of the project in year y, as calculated in Equations (11) and (12); P_i is the PV installed capacity of building i, in watts; C_{PV} is the PV cost, in CNY/W.

$$F_{\mathrm{cash},y} = R_{\mathrm{self-use}} + R_{\mathrm{export}} - \mathrm{AnnualMaintenanceCost} \tag{11}$$

$$\mathrm{AnnualMaintenanceCost} = \sum_{i=1}^{N} P_i \cdot C_{\mathrm{maintenance}} \tag{12}$$

where $R_{\mathrm{self-use}}$ is the revenue obtained by the building from the self-consumed PV generation, as calculated with Equation (13). R_{export} is the revenue earned from the PV generation exported to the grid, as calculated with Equation (14); $C_{\mathrm{maintenance}}$ is the unit cost of maintenance, which is 0.06 CNY/W.

$$R_{\mathrm{self-use}} = \sum_{i=1}^{N} \sum_{t=1}^{T} \left(E_{i,t}^{\mathrm{self}} \cdot T_{\mathrm{self-use}} \cdot r_{discount}\right) \tag{13}$$

$$R_{\mathrm{export}} = \sum_{i=1}^{N} \sum_{t=1}^{T} \left(E_{i,t}^{\mathrm{export}} \cdot T_{\mathrm{export}}\right) \tag{14}$$

where $T_{\mathrm{self-use}}$ is the electricity tariff. For residential buildings, this study adopts Shenzhen's peak-valley time-of-use tariff, as shown in Eq. (15) and Table 2. For industrial or commercial buildings, the tariff is fixed at 0.85 CNY/kWh. $r_{discount}$ is the electricity discount rate, set to 0.8. In distributed rooftop PV projects, generating revenue by supplying PV-generated electricity to buildings is a common practice, and an

Table 2
Time-of-use electricity tariff in Shenzhen.

Period	Time Range	Tariff (CNY/kWh)
Peak Hours	10:00-12:00, 14:00-19:00	1.10
Valley Hours	0:00-8:00	0.25
Off-peak hours	Remaining hours	0.65

electricity discount is often applied to offset rooftop rental costs.

$$T_{selfuse} = \begin{cases} T_{\text{valley}}, & \text{if } t \in \text{ValleyHours}, \\ T_{\text{peak}}, & \text{if } t \in \text{PeakHours}, \\ T_{\text{normal}}, & \text{otherwise}. \end{cases} \quad (15)$$

2.3.2. Algorithm parameters and decision-making strategy

The single- and multi-objective optimization algorithms are configured with consistent core parameters to ensure the stability and comparability of optimization results across different budget intervals. The base budget is defined as the total investment for full PV deployment across all buildings, with three budget intervals corresponding to different resource availability scenarios. Min-max normalization is applied in multi-objective optimization to eliminate dimension differences between indicators, ensuring fair non-dominated sorting by NSGA-II. Key algorithm parameters are standardized in Table 3.

3. Results

3.1. Case study setup

This study selected a building cluster in Shenzhen, China, as the case study. The building cluster consists of 245 buildings with a total rooftop area of 51,562 m^2. Fig. 5 illustrates the location of the case study area and the distribution of building types and heights. The cluster comprises a diverse mix of building functions: 202 low and mid-rise residential buildings (82.4 %), 10 high-rise residential buildings (4.1 %), 26 commercial buildings (10.6 %), and 7 industrial buildings (2.9 %). Building heights range from 13 to 178 meters, and individual rooftop areas vary from 7.5 to 2,053.7 m^2, reflecting significant heterogeneity in both form and scale.

3.2. Available areas identification results

Fig. 6a shows the simulation results of sunlight hours on the winter solstice. Fig. 6b illustrates the identification results of rooftop obstacles with buffer zones and maintenance pathways, which are combined into a single visualization due to their similar classification methods. Fig. 6c displays the integrated results of available rooftop area identification for the building cluster. The total available rooftop area is 23,982 m^2, while the unavailable rooftop area amounts to 27,580 m^2. The unavailable area arises from three overlapping sources: shadowed areas (20,767 m^2), rooftop obstacles (4,539 m^2), and maintenance pathways (16,999 m^2). Due to spatial overlaps among these categories, their summed area exceeds the actual total unavailable rooftop area. Together, these results establish a detailed rooftop availability map that serves as the geometric and operational input for subsequent PV layout generation.

Table 3
Parameter settings for the optimization and decision-making framework.

Parameter Category	Parameter	Value
Algorithm framework	Crossover probability	0.9
	Mutation probability	0.05
	Population size	200
	Number of generations	100
Parameter constraints	Budget interval	High (75 %–100 %), Medium (50 %–75 %), Low (25 %–50 %) of the base budget
	Decision variable type	Binary building-selection variable (0 = excluded, 1 = selected)
Fitness evaluation	Fitness function (single-objective)	Maximization of IRR / SSR / CEB
	Fitness function (multi-objective)	Maximization of normalized IRR, SSR, CEB (dimensionless)

3.3. Initial layout results

The initial layout generation module produced PV layouts for 198 out of 245 buildings, resulting in a total PV area of 20,403 m^2, while 47 buildings were excluded due to insufficient available rooftop space. Fig. 7a illustrates the initial layout results. As shown in Fig. 7b, the excluded buildings are generally associated with smaller rooftop areas, mostly below 150 m^2. Fig. 7c further indicates that these buildings have a substantially smaller mean rooftop area (33.13 m^2) compared to those with generated layouts (138.2 m^2). In addition, Fig. 7d shows that the excluded buildings exhibit higher proportions of all three categories of unavailable rooftop areas.

3.3.1. Environmental performance

Hourly electricity consumption and PV generation profiles were obtained through energy simulation based on the initial layout. Fig. 8a shows the hourly variations during the first year, illustrating the temporal profiles used for environmental performance assessment. Over a 10-year evaluation period, the total PV generation amounts to 61.61 GWh, which is translated into a cumulative CEB of 27,725.59 t CO_2.

3.3.2. Energy performance

All buildings are assumed to operate under a self-consumption plus grid-feed-in scheme. Based on the simulated PV generation and electricity consumption profiles, the self-sufficiency rate (SSR) was calculated to quantify energy performance. Fig. 8b presents the SSR variation on representative dates (March 1, June 1, September 1, and December 1). At the cluster scale, an annual SSR of 16.44 % is obtained for the first year.

3.3.3. Economic performance

Based on the initial layout and simulation results, the corresponding economic indicators were calculated. The initial layout requires a total investment of 15.63 million CNY, with an annual operation and maintenance cost of 0.31 million CNY. Over a 10-year assessment period, the resulting IRR is 14.61 %, and the net revenue amounts to 5.01 million CNY.

Overall, the initial layout generation module constructs module-level PV deployment configurations in a three-dimensional environment under geometric, shading, and operational constraints. These layouts translate available rooftop area into explicit deployment options and provide the spatial and data foundation required for subsequent optimization.

3.4. Optimization and decision-making results

3.4.1. Pareto frontier analysis and TOPSIS results

Fig. 9 presents the three- and two-dimensional distributions of feasible solutions, Pareto frontiers, and TOPSIS-optimal solutions under different budget intervals. The number of Pareto frontiers decreases with tighter budget constraints, from 209 in the high-budget interval to 36 and 25 in the medium and low intervals, respectively. Across all budget scenarios, feasible solutions exhibit structured distributions in the three-dimensional objective space, indicating clear trade-offs among SSR, IRR, and CEB. Taking the medium-budget scenario as an example, the Pareto-optimal solutions exhibit a trade-off among objectives: SSR ranges from 0.140 to 0.252, IRR from 12.5 % to 17.6 %, and CEB from 13770.58 to 21025.96 t CO_2, highlighting the competing nature of

Fig. 5. Case study area: location, building type distribution, and height variation.

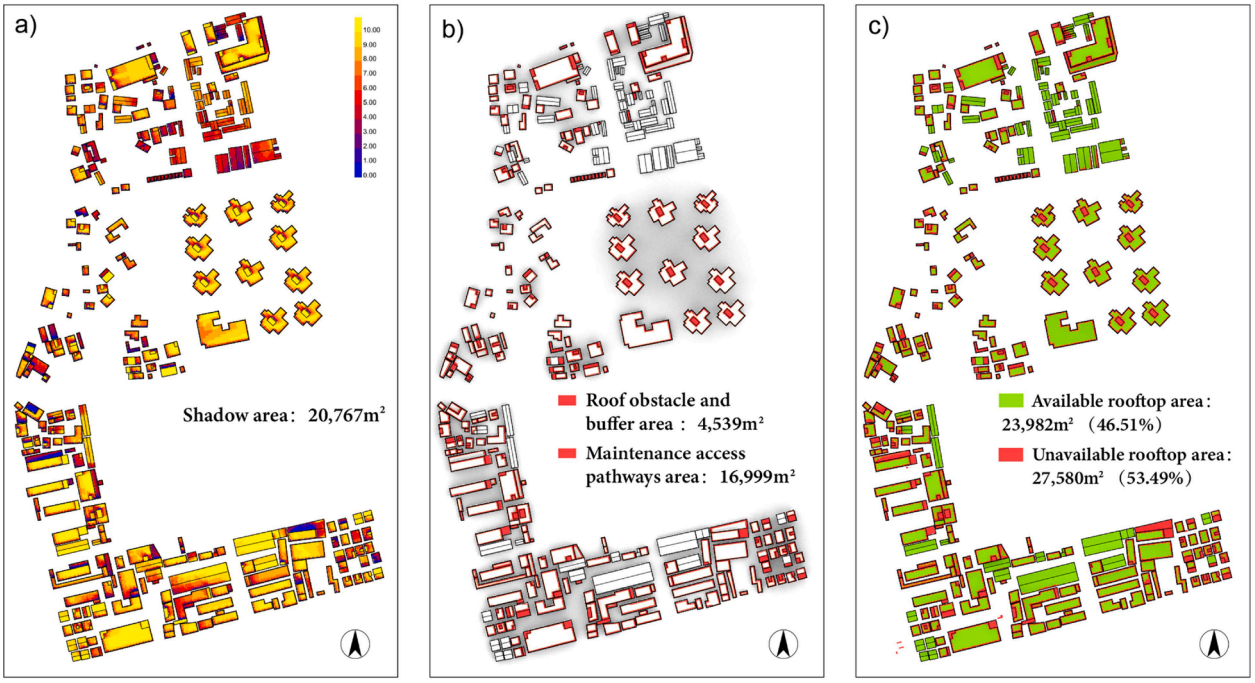

Fig. 6. Available areas identification results. a) simulation results of sunlight hours on the winter solstice. b) rooftop obstacles with buffer zones and maintenance pathways. c) integrated results of available rooftop area identification.

energy self-consumption, economic return, and environmental benefit. Regression analysis further quantifies these relationships. SSR and IRR show a positive correlation ($R^2 = 0.57$), while both indicators are negatively correlated with CEB, with R^2 values of 0.756 and 0.743, respectively. All correlations are statistically significant ($p < 0.001$).

Based on entropy-derived objective weights, TOPSIS is applied to identify a representative compromise solution within each budget interval. Table 4 reports the corresponding objective weights and closeness coefficients. Across budget intervals, the dominant objective weight varies: SSR receives the highest weight in the high and low budget intervals, whereas CEB becomes the highest-weighted objective in the medium budget interval. IRR remains the lowest-weighted objective in all intervals.

3.4.2. Performance of optimal solutions

Fig. 10a compares the core performance indicators of four representative solutions across low, medium, and high budget intervals. The IRR-optimal solution consistently achieves the highest internal rate of return, with values of 19.2 %, 17.6 %, and 16.1 % under low, medium, and high budgets, showing a decreasing trend as the budget level increases. The SSR-optimal solution yields the highest self-sufficiency rate in all scenarios, with SSR also decreasing as budget expands, indicating slightly reduced supply-demand matching at higher budget levels. For the CEB-optimal solution, total carbon emission reduction increases monotonically with budget expansion, reflecting the effect of larger deployment scales. In contrast, the TOPSIS-optimal solution exhibits intermediate but well-distributed performance across all three indicators, with each metric following the same trend as observed in the corresponding single-objective solutions. As shown in Fig. 10b, the radar plots indicate that TOPSIS solutions maintain a relatively balanced profile under different budget constraints, while achieving SSR levels close to those of the SSR-optimal solutions.

3.4.3. Comparison with randomly sampled solutions

A total of 30,000 random solutions were generated through unbiased random sampling, with each building having an equal probability of being selected. These solutions are approximately uniformly distributed across the predefined budget intervals. As shown in Fig. 11, the single-

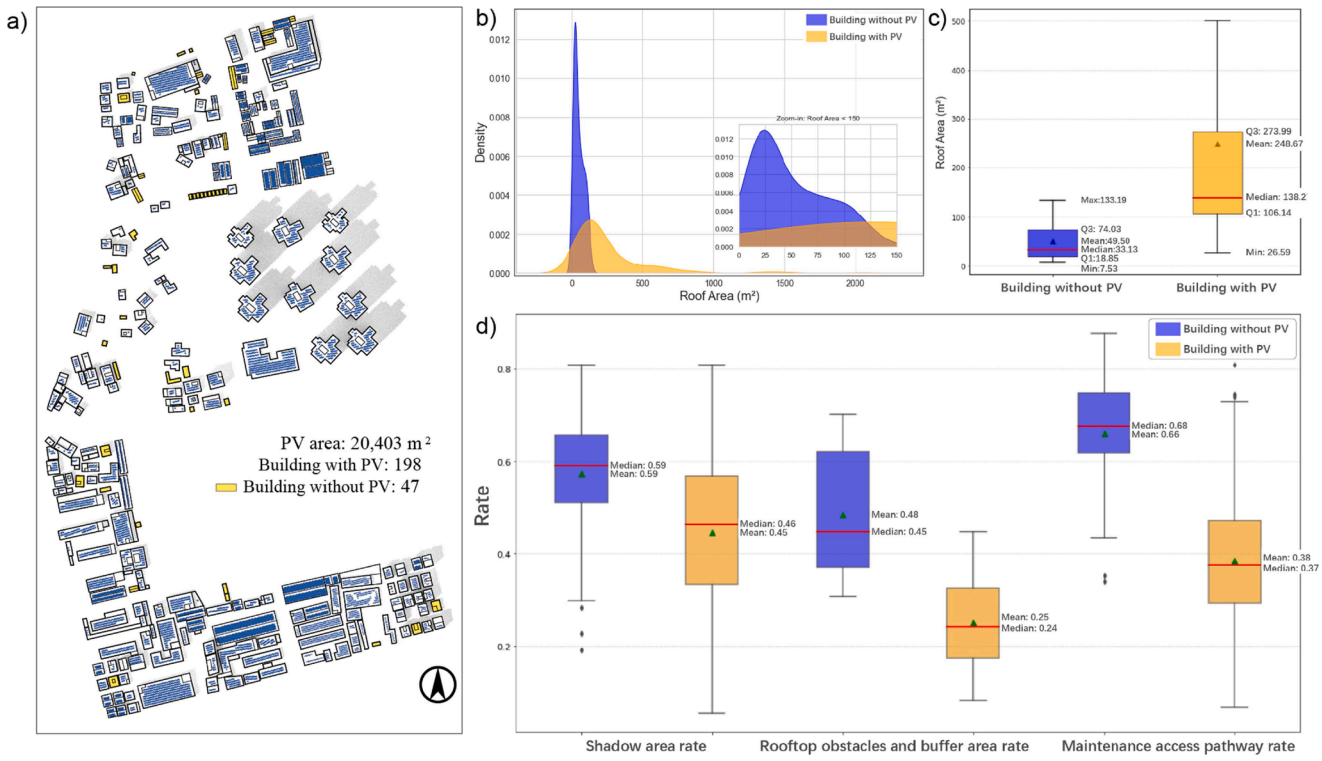

Fig. 7. Results of initial PV layout. a) initial layout. b) distribution of available rooftop area across buildings. c) comparison of rooftop areas between buildings with and without PV layouts. d) proportions of different categories of unavailable rooftop areas.

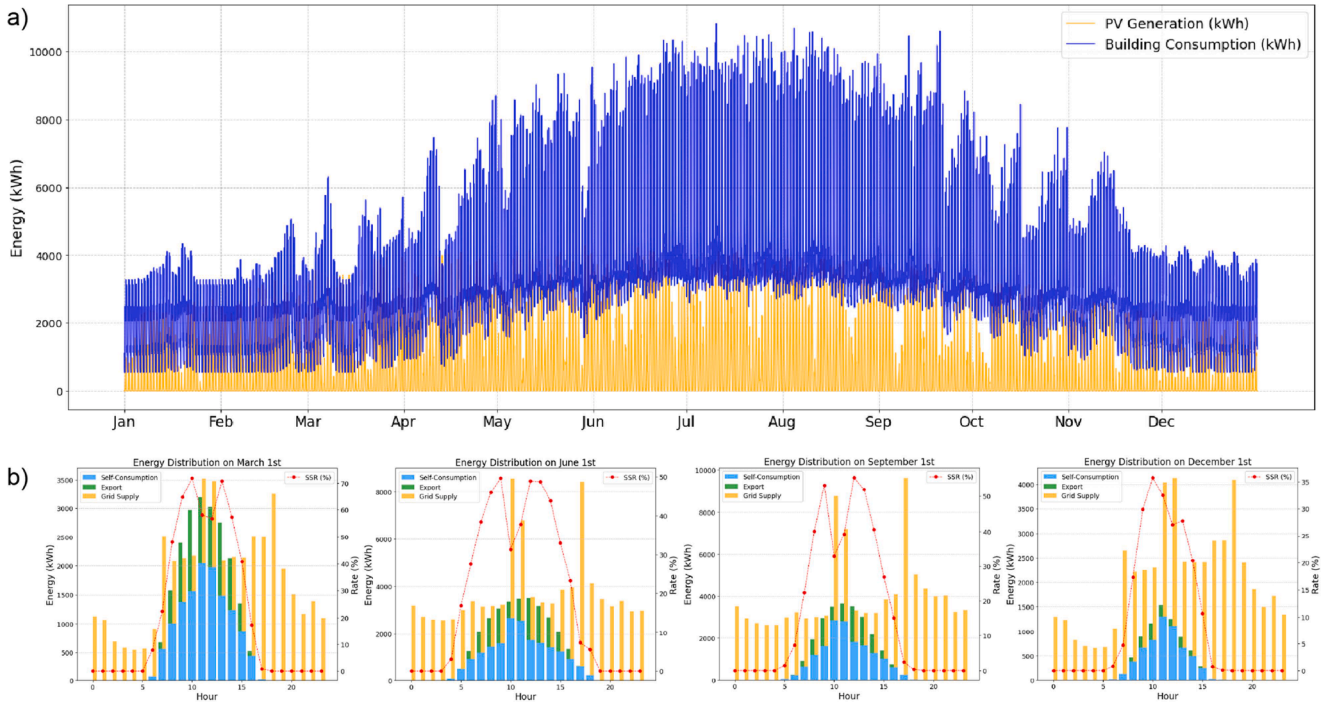

Fig. 8. Simulated energy performance of the initial PV layout. a) first-year hourly variations in electricity consumption and PV generation. b) diurnal variations in SSR on typical dates.

objective optimization solutions for IRR and SSR exceed the maximum values achieved by random sampling across all budget levels. In contrast, the best CEB obtained from single-objective optimization is comparable to the upper bound of the random solutions.

For the multi-objective optimization results, the TOPSIS-optimal solutions exhibit strict Pareto non-dominance with respect to all random solutions across the three budget intervals (Table 5). No random solution achieves an improvement in any objective without a simultaneous degradation in at least one other objective. Across all budget levels, the TOPSIS solutions achieve SSR values higher than the

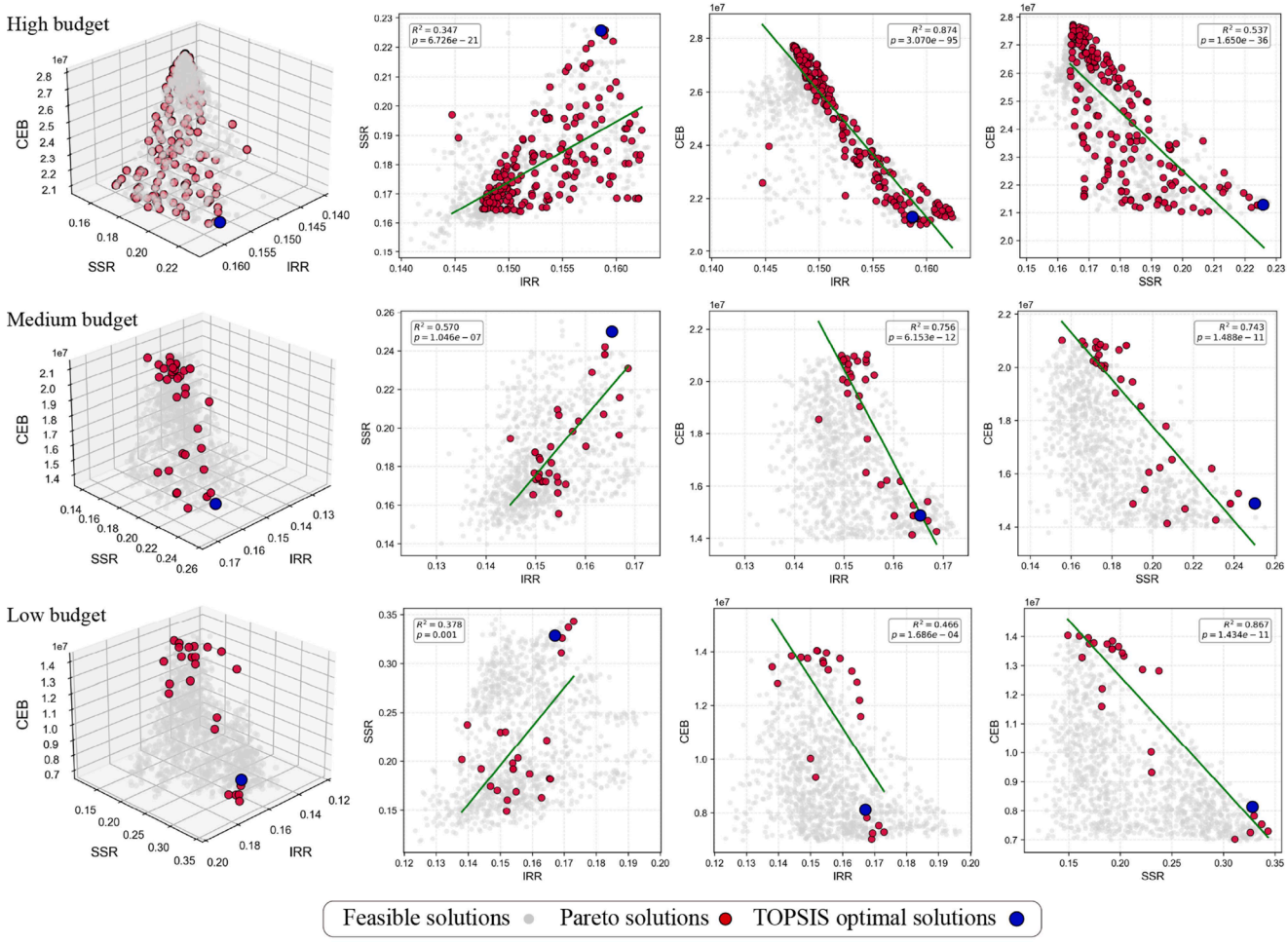

Fig. 9. Distribution of feasible solutions and Pareto-optimal fronts in the three-objective optimization under different budget constraints.

Table 4
Entropy weights, stability ratios and TOPSIS closeness coefficients under different budget intervals.

Budget Interval	Weight of IRR	Weight of SSR	Weight of CEB	TOPSIS Closeness Coefficient
High	0.181	0.523	0.295	0.700
Medium	0.273	0.354	0.374	0.588
Low	0.219	0.470	0.311	0.701

maximum obtained from random sampling, while their IRR values remain higher than most random solutions.

3.4.4. *Preference of optimization strategies*

Fig. 12a illustrates the number of selected buildings and the corresponding budget utilization for the four optimal solutions under different budget constraints. The CEB-optimal solution consistently operates close to the upper budget limit and selects the largest number of buildings, including all available buildings under the high-budget constraint. In contrast, the IRR-optimal and SSR-optimal solutions tend to select fewer buildings, resulting in lower budget utilization. The TOPSIS-selected solution also involves a relatively small number of buildings but exhibits higher budget utilization than the single-objective IRR and SSR solutions.

Fig. 12b compares two key building characteristics, namely roof area and energy intensity, for each solution across budget intervals. Energy intensity is defined as the ratio of first-year PV generation to rooftop area. Under the low-budget constraint, pronounced differences are observed among optimization strategies. The CEB-optimal solution consistently selects buildings with relatively small roof areas and low energy intensity, exhibiting the smallest average roof area of no more than 125 m^2 and the lowest energy intensity of no more than 92.05 kWh/m^2. In contrast, the IRR-optimal solution shows substantially higher values for both indicators, with an average roof area of at least 426.66 m^2 and an energy intensity of at least 138.99 kWh/m^2. In the medium and high budget scenarios, the TOPSIS-optimal solution presents relatively higher roof area and energy intensity compared to other solutions, although these differences are not statistically significant.

Fig. 13 shows the deployment results of the four strategies under the low-budget scenario, with buildings selected by multiple strategies specifically marked; only two buildings are chosen by all four strategies and nine are selected by any three, indicating low overlap and distinct selection preferences across objectives.

3.5. *Sensitivity analysis*

3.5.1. *Sensitivity analysis results for initial layout generation*

Sensitivity tests were performed to examine the influence of two key geometric parameters, namely the offset range and the expansion ratio, on the initial layout generation stage. The tests were conducted under controlled conditions: a fixed random seed, layout generation on 20 randomly selected buildings, and all other parameters held constant. The results are summarized in Table 6. For the expansion ratio, the maximum panel count was attained at 10 %. Any further increase in the ratio only resulted in longer computational time without additional gains in panel quantity. For the offset range, computational duration

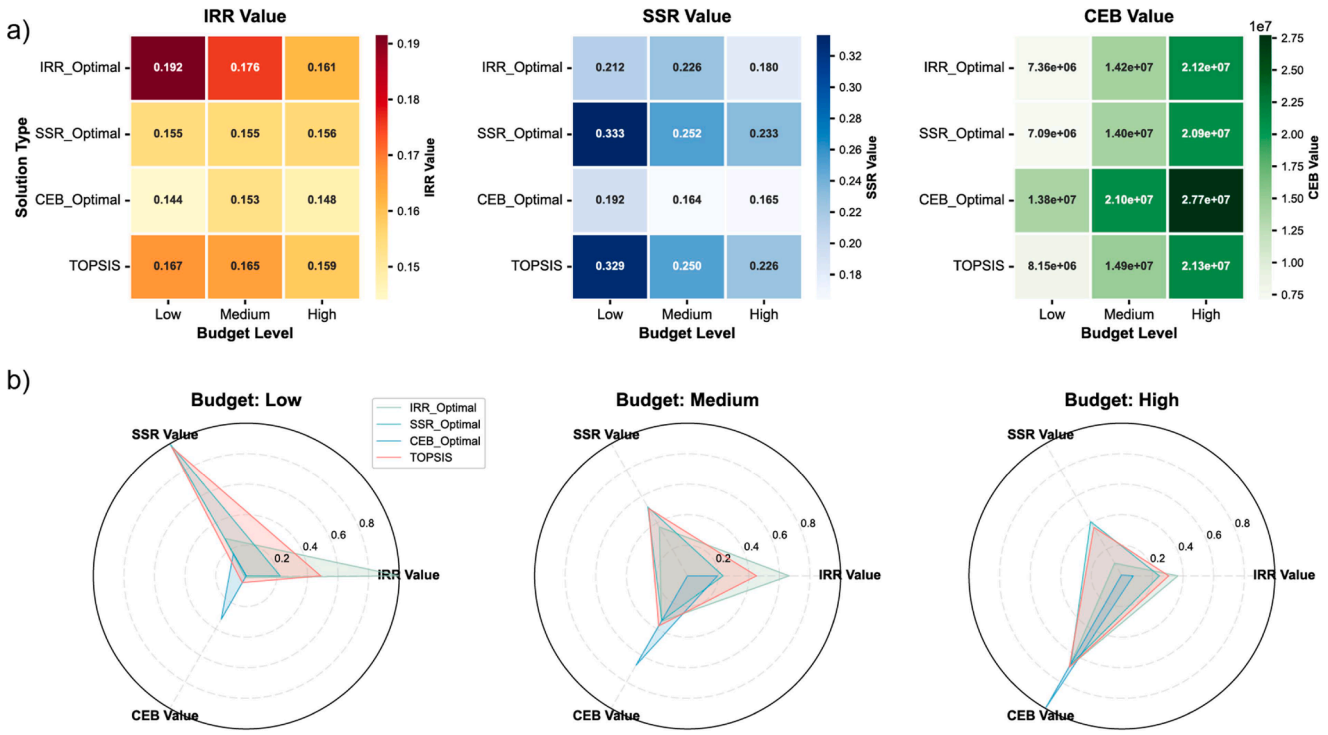

Fig. 10. Performance comparison of representative optimal solutions under different budget intervals. a) indicator values of IRR-optimal, SSR-optimal, CEB-optimal, and TOPSIS-optimal solution. b) radar plots of normalized multi-indicator performance grouped by budget interval.

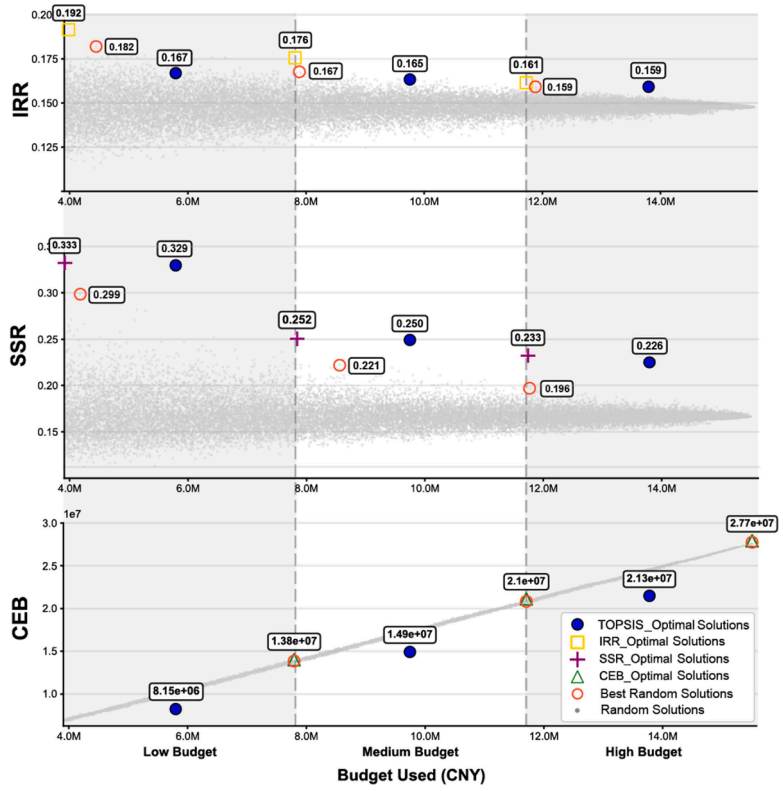

Fig. 11. Comparison between optimization solutions and randomly sampled solutions under different budget intervals.

remained stable, while the panel count increased and reached its maximum when the range expanded to ±5 m. Thus, a 10 % expansion ratio and a ±5 m offset range were selected as optimal parameters, achieving the maximum panel count without additional computational overhead.

3.5.2. *Sensitivity analysis of entropy-weighted TOPSIS decision-making*

To assess the robustness of the multi-objective decision-making

Table 5
Performance comparison between the TOPSIS-selected solution and randomly sampled solutions under different budget intervals.

Comparison Aspect	Metric	Low Budget	Medium Budget	High Budget
Random solution set	**Number of random solutions within the budget interval**	9900	9937	10163
	Number of random solutions that strictly dominate the TOPSIS solution	0	0	0
Single-indicator comparison	Proportion of random solutions outperformed by the TOPSIS solution (IRR, %)	98.5	99.9	100
	SSR (%)	100	100	100
	CEB (%)	17.4	13.2	4.6

process, a sensitivity analysis was conducted on the entropy-derived objective weights used in the TOPSIS evaluation. The analysis focuses on whether small perturbations in weight allocation would lead to different optimal solution selections. Specifically, the baseline entropy weights were subjected to random perturbations within ±10 %. For each budget interval, the perturbation process was repeated 100 times, and the TOPSIS optimal solution was re-identified in each trial. The results, summarized in Table 7, indicate that the stability ratio remains high across all budget intervals (≥0.83), demonstrating that the TOPSIS-optimal solutions are insensitive to moderate weight variations. This confirms the robustness of the entropy-weighted TOPSIS decision-making process and supports the reliability of the reported multi-objective optimal solutions.

3.5.3. *Sensitivity analysis results for optimization and decision-making*

To examine the performance of the proposed optimization

Table 6
Sensitivity analysis of geometric parameters in initial layout generation.

Parameter type	Parameter value	Number of panels	Total duration (s)
Expansion ratio	0 %	490	150.62
	10 %	494	173.55
	25 %	492	210.18
	50 %	494	289.62
	100 %	492	477.89
Offset range (±m)	1	476	172.38
	2	484	172.48
	5	494	172.93
	10	494	172.97
	15	494	172.22

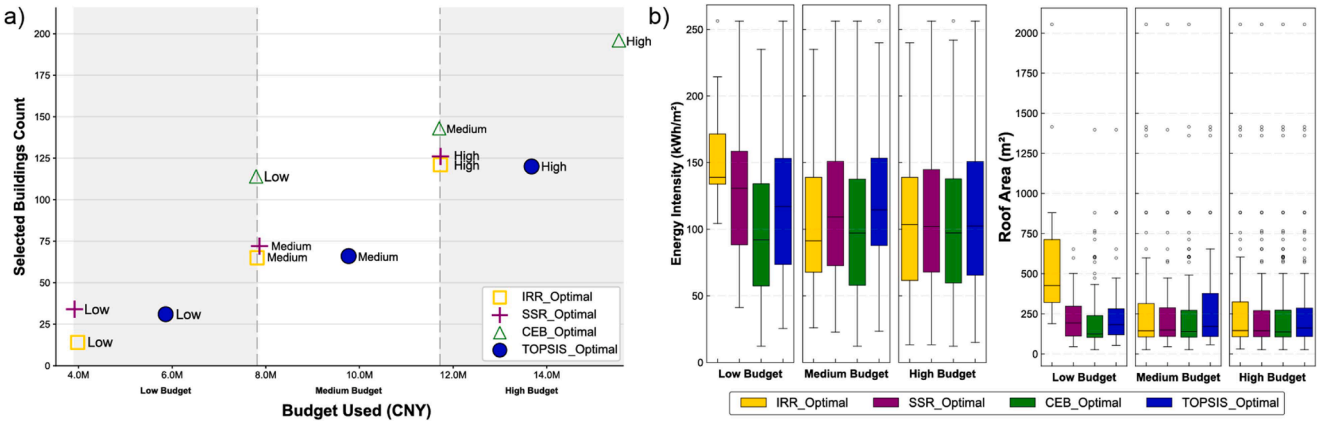

Fig. 12. Building selection characteristics of different optimization strategies under varying budget constraints. a) number of selected buildings and budget utilization. b) roof area and energy intensity of selected buildings.

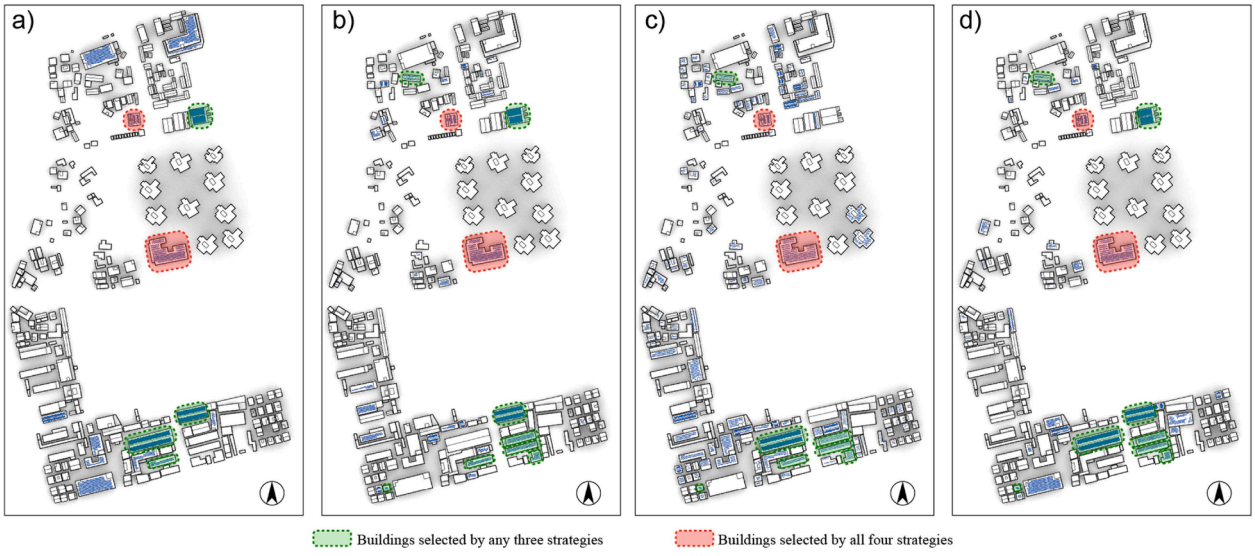

Fig. 13. Rooftop PV deployment results under the low-budget constraint. a) CEB-optimal. b) IRR-optimal. c) SSR-optimal. d) TOPSIS-optimal.

Table 7
Stability of the TOPSIS decision under different budget levels.

Budget level	Number of Pareto solutions	Stability ratio*
Low	25	100 %
Medium	36	83 %
High	209	100 %

* Stability ratio is defined as the proportion of weight-perturbation trials in which the TOPSIS-selected optimal solution remains unchanged.

framework under parameter variations, sensitivity analyses were conducted for two key parameters: feed-in tariff price and PV module efficiency. Based on realistic ranges observed in practice, both parameters were perturbed by ±10 %, and the medium-budget interval was selected as the representative test scenario. For single-objective optimization with IRR as the target metric, Fig. 14 shows that the IRR-optimized solutions consistently exceed the best-performing random solutions under all tested variations of feed-in tariff and PV module efficiency. At the multi-objective level, the TOPSIS-selected solutions exhibit robust performance under all parameter perturbations, consistently outperforming the majority of random solutions in at least two objectives (Table 8).

4. Discussion

4.1. Rooftop area availability assessment based on spatial constraints

Compared with conventional utilization-factor approaches, which typically assume that 60 % or more of rooftop areas are suitable for PV installation in dense urban contexts (Wang et al., 2022, Yuan et al., 2016), the available rooftop proportion identified in this study is substantially lower at 46.51 %. This highlights the importance of explicit rooftop-level modeling that accounts for shading, rooftop obstacles, and maintenance access requirements, leading to a more conservative but realistic estimation of deployable PV potential. Shadow areas and mandatory maintenance pathways constitute the largest shares of excluded rooftop areas, indicating that urban morphology and

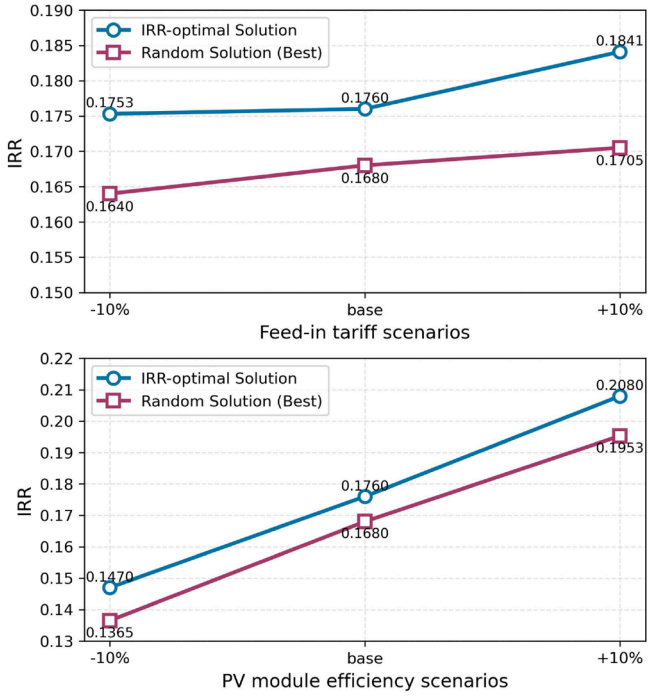

Fig. 14. Sensitivity analysis of optimized solutions compared with random sampling benchmarks.

Table 8
Single-indicator superiority of the TOPSIS solution under parameter perturbations.

Parameter category	Scenario	IRR (%)	SSR (%)	CEB (%)
Electricity price	−10 %	100*	99.9	19.8
	Base	99.9	100	13.2
	10 %	91.1	100	42.7
PV efficiency	−10 %	74.9	97.5	88.5
	Base	99.9	100	13.2
	10 %	62.5	95.1	98.3

* Values indicate the proportion of randomly sampled solutions that are outperformed by the TOPSIS-soptimal solution for each individual indicator.

regulatory constraints play a dominant role in limiting rooftop PV deployment. The spatial overlap among exclusion categories further suggests that integrated rooftop and architectural design, such as coordinating equipment placement with access routes or optimizing roof geometry, may enhance rooftop PV potential.

4.2. Implications of optimization strategy comparison

The comparison among single-objective optimization, multi-objective optimization, and random sampling underscores the importance of optimization strategy selection in rooftop PV deployment. Single-objective approaches consistently outperform random sampling in their targeted metric, confirming their effectiveness when a specific performance priority is predefined. However, they inevitably sacrifice non-optimized objectives, limiting their suitability in contexts requiring balanced outcomes. For instance, Ren et al. (2023) used an ILP-based strategy to compare heuristics prioritizing either total solar potential or rooftop energy intensity, showing that single-criterion optimization often compromises overall generation efficiency or cost-effectiveness. In contrast, strategies that explicitly balance competing objectives yield more robust system-level performance. Notably, the TOPSIS-optimal solutions maintain stable, non-inferior performance across all budget scenarios and outperform most random solutions in at least two objectives, demonstrating the advantage of the proposed hybrid framework in delivering balanced, decision-relevant outcomes under realistic budget constraints.

4.3. Framework design and practical applicability

The proposed hybrid optimization framework integrates 3D layout generation with subsequent single- and multi-objective optimization, effectively decoupling physical feasibility assessment from performance driven decision-making. By first translating available rooftop areas into explicit, constructible PV configurations, the framework ensures engineering realism and provides a spatially accurate basis for energy, environmental, and economic evaluations. The use of binary building-level selection variables separates layout generation from system-scale optimization, avoiding direct operations on complex 3D platforms and significantly reducing computational complexity. This modular design enables single-objective runs to explore performance extremes under strict budget constraints, while multi-objective TOPSIS-based selection identifies balanced trade-offs across all objectives. As demonstrated in the Shenzhen case study, the approach supports flexible adaptation to varying budget scenarios, heterogeneous building characteristics, and evolving policy priorities, offering a scalable and practical pathway for cluster-scale rooftop PV deployment planning.

4.4. Limitations and potential future work

Despite the advantages of the proposed framework, several limitations remain. First, the rooftop area identification module has limited adaptability to complex or highly irregular roof geometries and currently relies on manual input, which constrains automation and

scalability. Second, each objective dimension in this study is represented by a single indicator (IRR, SSR, CEB), potentially overlooking other relevant performance aspects. Third, the current framework does not consider energy storage integration, which could affect self-consumption and system flexibility.

Future research could address these limitations by integrating satellite imagery and shadow simulation to automate and accelerate rooftop availability assessment, reducing reliance on manual modeling. Additionally, incorporating energy storage and expanding the set of performance indicators would enable more comprehensive multi-objective optimization, supporting enhanced planning and decision-making for large-scale rooftop PV deployment.

5. Conclusion

In this study, a three-module rooftop PV layout generation and optimization model is proposed to enhance the efficiency of PV layout planning for large-scale building cluster. The first module identifies unsuitable zones in three categories to precisely delineate available rooftop areas. The second module employs a genetic algorithm within a parametric 3D modeling environment, incorporating practical PV deployment constraints to generate an initial layout with a maximum number of PV panels. Based on this, the third module implements a hybrid single- and multi-objective optimization framework via binary programming. By conducting a case study containing 245 real rooftops in a high-density urban district of Shenzhen, the following major conclusions were made.

1) The available area identification module determines viable PV installation areas by explicitly excluding three types of unavailable zones: shadowed regions, roof obstacles with surrounding buffer zones, and maintenance access pathways. Applied to the 245-building cluster with a total rooftop area of 51,562 m^2, the module identified 23,982 m^2 of technically usable area, yielding an available area ratio of 46.51 %. This is lower than typical utilization-factor assumptions, demonstrating that the proposed method provides a more accurate and conservative basis for practical PV deployment planning.
2) The initial layout generation module produces three-dimensional, engineering-feasible PV layouts by translating available rooftop areas into explicit deployment configurations. Feasible layouts were generated for 198 buildings, yielding a total installed PV area of 20,403 m^2. These layouts provide the spatial and data foundation required for subsequent energy, economic, and environmental performance evaluation, enabling optimization analyses.
3) Comparison with 30,000 randomly sampled solutions demonstrates the superiority of the proposed optimization framework. Single-objective optimization solutions for IRR and SSR consistently outperform the best random solutions, while CEB-optimal solutions reach comparable maxima. Multi-objective TOPSIS-optimal solution maintains a well-balanced performance across all three indicators, showing Pareto non-inferiority relative to the random solutions.
4) The optimal solutions exhibit clear trends with increasing budget: IRR and SSR decrease while CEB increases. Specifically, the IRR-optimal solution declines from 19.2 % to 16.1 %, and the SSR-optimal solution drops from 33.3 % to 23.3 % as the budget rises. The CEB-optimal solution prioritizes selecting many small, low-cost rooftops, whereas the IRR- and SSR-optimal solutions focus on larger, higher energy-intensity rooftops. The TOPSIS-optimal solutions balance these tendencies, with multi-objective weighting reflecting a higher priority on SSR in the high- and low-budget scenarios, and assigning the highest weight to CEB in the medium-budget scenario.

In conclusion, the proposed PV layout generation and optimization model can be used in practice to improve rooftop PV deployment for large-scale building cluster, promoting urban decarbonization and sustainable development.

Data availability

The data that support the findings of this study are available from the corresponding author upon reasonable request.

CRediT authorship contribution statement

Rui Miao: Writing – original draft, Validation, Methodology, Conceptualization. **Haoqing Zhu:** Writing – review & editing. **Yi Zhang:** Writing – review & editing, Supervision, Methodology, Funding acquisition, Conceptualization. **Kanghua Li:** Visualization, Software. **Yuan Yuan:** Writing – review & editing, Methodology. **Pengyuan Shen:** Resources, Methodology. **He Qi:** Resources, Methodology.

Declaration of competing interest

The authors declare that they have no known competing financial interests or personal relationships that could have appeared to influence the work reported in this paper.

Acknowledgments

This research was supported Shenzhen Science and Technology Program KCXST20221021111608020; Research and Development Project of Ministry of Housing and Urban-Rural Development of the People's Republic China (Grant No. 2022-K-121).

Data availability

Data will be made available on request.

References

Allouhi, A. (2020). Solar PV integration in commercial buildings for self-consumption based on life-cycle economic/environmental multi-objective optimization. *Journal of Cleaner Production, 270*, Article 122375. https://doi.org/10.1016/j.jclepro.2020.122375. Oct.

Arce, M. Elena, Saavedra, Á., Míguez, J. L., & Granada, E. (2015). The use of grey-based methods in multi-criteria decision analysis for the evaluation of sustainable energy systems: A review. *Renewable and Sustainable Energy Reviews, 47*, 924–932. https://doi.org/10.1016/j.rser.2015.03.010. July.

Bahaj, A. S. (2003). Photovoltaic roofing: issues of design and integration into buildings. *Renewable Energy, 28*(14), 2195–2204. https://doi.org/10.1016/S0960-1481(03)00104-6. Nov.

Barbón, A., Ghodbane, M., Bayón, L., & Said, Z. (2022). A general algorithm for the optimization of photovoltaic modules layout on irregular rooftop shapes. *Journal of Cleaner Production, 365*, Article 132774. https://doi.org/10.1016/j.jclepro.2022.132774. Sept.

Bayod-Rújula, A. A., Ortego-Bielsa, A., & Martínez-Gracia, A. (2011). Photovoltaics on flat roofs: Energy considerations. *Energy, 36*(4), 1996–2010. https://doi.org/10.1016/j.energy.2010.04.024. Apr.

BJX. (2025). In 2025, PERC-210 products accounted for nearly 60% of output, reshaping the competitive landscape of the market. https://guangfu.bjx.com.cn/news/20250122/1424075.shtml accessed Dec 01, 2025.

Breyer, C., Koskinen, O., & Blechinger, P. (2015). Profitable climate change mitigation: The case of greenhouse gas emission reduction benefits enabled by solar photovoltaic systems. *Renewable and Sustainable Energy Reviews, 49*, 610–628. https://doi.org/10.1016/j.rser.2015.04.061. Sept.

Cao, Z., Liu, Y., Bai, Y., Wang, Y., Ye, S., & Cao, H. (2024). Study on the optimal layout of roof vents and rooftop photovoltaic of the industrial workshop. *Building and Environment, 260*, 111624. https://doi.org/10.1016/j.buildenv.2024.111624.

Chapman, B., Jost, G., & van der Pas, R. (2007). *Using OpenMP: Portable shared memory parallel programming (Scientific and Engineering Computation)*. The MIT Press.

Chen, Z., et al. (2022). Assessing the potential and utilization of solar energy at the building-scale in Shanghai. *Sustainable Cities and Society, 82*, Article 103917. https://doi.org/10.1016/j.scs.2022.103917. July.

Chen, X. M., Li, Y., Zhao, B. Y., & Wang, R. Z. (2020). Are the optimum angles of photovoltaic systems so important? *Renewable and Sustainable Energy Reviews, 124*, Article 109791. https://doi.org/10.1016/j.rser.2020.109791. May.

Cuesta-Fernández, I., Vargas-Salgado, C., Alfonso-Solar, D., & Gómez-Navarro, T. (2023). "The contribution of metropolitan areas to decarbonize the residential stock in Mediterranean cities: A GIS-based assessment of rooftop PV potential in Valencia,

Spain. *Sustainable Cities and Society, 97*, Article 104727. https://doi.org/10.1016/j.scs.2023.104727. Oct.
Deb, K., Pratap, A., Agarwal, S., & Meyarivan, T. (2002). A fast and elitist multiobjective genetic algorithm: NSGA-II. *IEEE Transactions on Evolutionary Computation, 6*(2), 182–197. https://doi.org/10.1109/4235.996017. Apr.
Deng, X., Zhang, Y., Zhang, Y., & Qi, H. (2022). Toward Smart Multizone HVAC Control by Combining Context-Aware System and Deep Reinforcement Learning. *IEEE Internet of Things Journal, 9*(21), 21010–21024. https://doi.org/10.1109/JIOT.2022.3175728. Nov.
EE Power. (2024). Understanding PV System Standards, Ratings, and Test Conditions - Technical Articles. https://eepower.com/technical-articles/understanding-pv-system-standards-ratings-and-test-conditions/ accessed Dec 23, 2024.
EnergyPlus. (2024). EnergyPlus. https://energyplus.net/ accessed Dec 08, 2024.
Gao, D., et al. (2025). Multi-objective optimization of urban industrial building rooftop PV-storage systems: Integrating dynamic degradation and lifecycle carbon footprint. *Sustainable Cities and Society, 130*, Article 106615. https://doi.org/10.1016/j.scs.2025.106615. July.
Google. (2024). Google Maps. https://www.google.co.jp/maps accessed Dec 21, 2024.
Hafez, A. Z., Soliman, A., El-Metwally, K. A., & Ismail, I. M. (2017). Tilt and azimuth angles in solar energy applications – A review. *Renewable and Sustainable Energy Reviews, 77*, 147–168. https://doi.org/10.1016/j.rser.2017.03.131. Sept.
Holland, J. H. (1992). *Adaptation in Natural and Artificial Systems: An Introductory Analysis with Applications to Biology, Control, and Artificial Intelligence*. MIT Press.
Hwang, C.-L., & Yoon, K. (1981). *Multiple attribute decision making: Methods and applications : a State-of-the-art Survey*. Springer-Verlag.
Jelle, B. P. (2013). The challenge of removing snow downfall on photovoltaic solar cell roofs in order to maximize solar energy efficiency—Research opportunities for the future. *Energy and Buildings, 67*, 334–351. https://doi.org/10.1016/j.enbuild.2013.08.010. Dec.
R. E. Kontar and X. Jin, "Optimal efficiency and operational cost savings: A framework for automated rooftop Pv placement," 2020.
Kucuksari, S., et al. (2014). An Integrated GIS, optimization and simulation framework for optimal PV size and location in campus area environments. *Applied Energy, 113*, 1601–1613. https://doi.org/10.1016/j.apenergy.2013.09.002. Jan.
Ladybug Tools. (2024). Ladybug Tools. https://www.ladybug.tools/ accessed Dec 08, 2024.
Ladybug Tools. (2025). EPW Map. https://www.ladybug.tools/epwmap/ accessed Jan 22, 2025.
Lawrence Berkeley National Laboratory (LBNL). (2025). https://eta.lbl.gov/news/china-s-opportunity-80-clean-power.
Lee, M., Hong, T., Jeong, J., & Jeong, K. (2018). Development of a rooftop solar photovoltaic rating system considering the technical and economic suitability criteria at the building level. *Energy, 160*, 213–224. https://doi.org/10.1016/j.energy.2018.07.020. Oct.
Li, Y., Li, H., Miao, R., Qi, H., & Zhang, Y. (2023). Energy–Environment–economy (3E) analysis of the performance of introducing photovoltaic and energy storage systems into residential buildings: A case study in Shenzhen, China. *Sustainability, 15*(11), 9007. https://doi.org/10.3390/su15119007. June.
Liu, K., Xu, X., Huang, W., Zhang, R., Kong, L., & Wang, X. (2023). A multi-objective optimization framework for designing urban block forms considering daylight, energy consumption, and photovoltaic energy potential. *Building and Environment, 242*, Article 110585. https://doi.org/10.1016/j.buildenv.2023.110585. Aug.
Longi. (2025). The World's Leading Supplier of Solar PV Solutions. https://www.longi.com/us/ accessed Dec 09, 2024.
Ma, L., et al. (2016). Multi-party energy management for smart building cluster with PV systems using automatic demand response. *Energy and Buildings, 121*, 11–21. https://doi.org/10.1016/j.enbuild.2016.03.072. June.
Ma, Z., et al. (2023). Shading effect and energy-saving potential of rooftop photovoltaic on the top-floor room. *Solar Energy, 265*, Article 112099. https://doi.org/10.1016/j.solener.2023.112099. Nov.
Robert McNeel & Associates. (2024). Grasshopper. https://www.grasshopper3d.com/. accessed Dec 08, 2024.
Meng, B., Loonen, R. C. G. M., & Hensen, J. L. M. (2020). Data-driven inference of unknown tilt and azimuth of distributed PV systems. *Solar Energy, 211*, 418–432. https://doi.org/10.1016/j.solener.2020.09.077. Nov.
Ministry of Ecology and Environment of China (MEE). (2025). Announcement on the release of 2022 carbon dioxide emission factors for electricity. https://www.mee.gov.cn/xxgk2018/xxgk/xxgk01/202412/t20241226_1099413.html accessed Feb 10, 2025.
Ministry of Housing and Urban-Rural Development of the People's Republic of China. (2024).https://www.mohurd.gov.cn/gongkai/zc/wjk/art/2012/art_17339_211716.html.accessed Dec 10, 2024.
Nassar, Y. F., Alsadi, S. Y., Ali, K. A., Yousef, A. H., & Fakher, M. A. (2019). Numerical analysis and optimization of area contribution of The PV cells in the PV/T flat-plate solar air heating collector. *Journal of Solar Energy Research Updates, 6*, 43–50. https://doi.org/10.31875/2410-2199.2019.06.5. Jan.
Nassar, Y. F., El-Khozondar, H. J., Belhaj, S. O., Alsadi, S. Y., & Abuhamoud, N. M. (2022). View factors in horizontal plane fixed-mode solar PV fields. *Frontiers in Energy Research, 10*, Article 859075.
Nassar, Y., et al. (2025). Towards green economy: case of electricity generation sector in Libya. *Solar Energy and Sustainable Development, 14*, 334–360. https://doi.org/10.51646/jsesd.v14i1.549. Apr.
Nassar, Y. F., et al. (2025). Estimation of CO2 emission within Libya's electricity generation sector. *Next Research, 2*(3), Article 100567. https://doi.org/10.1016/j.nexres.2025.100567. Sept.
Nassar, Y. F., et al. (2025). Regression model for optimum solar collectors' tilt angles in Libya. In *2023 8th International Engineering Conference on Renewable Energy & Sustainability (ieCRES)* (pp. 1–6). IEEE, 2023Accessed: Dec. 01[Online]. Available https://ieeexplore.ieee.org/abstract/document/10209547/.
Nassar, Y. F., Belhaj, S., Alsadi, S. Y., & El-Khozondar, H. J. (2022). Analysis of the view factors in rooftop PV solar. In *2022 3rd International Conference on Smart Grid and Renewable Energy (SGRE)* (pp. 1–6). https://doi.org/10.1109/SGRE53517.2022.9774104. Mar.
Odeh, S., & Nguyen, T. H. (2021). Assessment method to identify the potential of rooftop PV systems in the residential districts. *Energies, 14*(14), Article 14. https://doi.org/10.3390/en14144240. ArtJan.
OpenStreetMap. (2024). OpenStreetMap database. https://www.openstreetmap.org/ accessed Dec 08, 2024.
Pan, D., Bai, Y., Chang, M., Wang, X., & Wang, W. (2022). The technical and economic potential of urban rooftop photovoltaic systems for power generation in Guangzhou, China. *Energy and Buildings, 277*, Article 112591. https://doi.org/10.1016/j.enbuild.2022.112591. Dec.
Paydar, M. Akbari (2020). Optimum design of building integrated PV module as a movable shading device. *Sustainable Cities and Society, 62*, Article 102368. https://doi.org/10.1016/j.scs.2020.102368. Nov.
R. M. & Associates. (2025). Rhinoceros 3D," Accessed: Jan. 22 www.rhino3d.com https://www.rhino3d.com/cn/japan/ Accessed: Jan. 22[Online]. Available.
Ren, H., Ma, Z., Chan, A. B., & Sun, Y. (2023). Optimal planning of municipal-scale distributed rooftop photovoltaic systems with maximized solar energy generation under constraints in high-density cities. *Energy, 263*, Article 125686. https://doi.org/10.1016/j.energy.2022.125686. Jan.
REN21. (2025). Renewables 2025 Global Status Report (GSR). https://www.ren21.net/gsr-2025/technologies/solar-pv/ accessed Jan 07, 2025.
Rutten, D., Groups, V. (2024). Galapagos. https://www.grasshopper3d.com/groups/group/show?groupUrl=galapagos accessed Dec 23, 2024.
Santos, T., Gomes, N., Freire, S., Brito, M. C., Santos, L., & Tenedório, J. A. (2014). Applications of solar mapping in the urban environment. *Applied Geography, 51*, 48–57. https://doi.org/10.1016/j.apgeog.2014.03.008. July.
Šimić, Z., Topić, D., Crnogorac, I., & Knežević, G. (2021). Method for sizing of a PV system for family home using economic indicators. *Energies, 14*(15), 4529. https://doi.org/10.3390/en14154529. Jan.
Solemma. (2025). ClimateStudio. https://www.solemma.com/climatestudio accessed Jan 22, 2025.
Stenabaugh, S. E., Iida, Y., Kopp, G. A., & Karava, P. (2015). Wind loads on photovoltaic arrays mounted parallel to sloped roofs on low-rise buildings. *Journal of Wind Engineering and Industrial Aerodynamics, 139*, 16–26. https://doi.org/10.1016/j.jweia.2015.01.007. Apr.
Sun, B., Yu, Y., & Qin, C. (2017). Should China focus on the distributed development of wind and solar photovoltaic power generation? A comparative study. *Applied Energy, 185*, 421–439. https://doi.org/10.1016/j.apenergy.2016.11.004. Jan.
Talavera, D. L., Nofuentes, G., & Aguilera, J. (2010). The internal rate of return of photovoltaic grid-connected systems: A comprehensive sensitivity analysis. *Renewable Energy, 35*(1), 101–111. https://doi.org/10.1016/j.renene.2009.07.006. Jan.
Tao, Q., Tantet, A., Badosa, J., Cros, S., & Drobinski, P. (2025). Multiple-scale distributed PV potential penetration in a densely populated city: A case study of Grand Paris metropolis. *Sustainable Cities and Society, 122*, Article 106232. https://doi.org/10.1016/j.scs.2025.106232. Mar.
Tian, J., & Ooka, R. (2025). Prediction of building-scale solar energy potential in urban environment based on parametric modelling and machine learning algorithms. *Sustainable Cities and Society, 119*, Article 106057. https://doi.org/10.1016/j.scs.2024.106057. Feb.
UNFCCC. (2015). Adoption of the Paris Agreement. Proposal by the President. https://unfccc.int/documents/9064. accessed July 15, 2024.
Verma, S., Pant, M., & Snasel, V. (2021). A Comprehensive Review on NSGA-II for Multi-Objective Combinatorial Optimization Problems. *IEEE Access, 9*, 57757–57791. https://doi.org/10.1109/ACCESS.2021.3070634
Wang, M., Jia, Z., & Xiang, C. (2025). Multi-objective optimization design of high-rise high-density urban morphology and their multidimensional assessment of PV capacity. *Sustainable Cities and Society, 130*, Article 106601. https://doi.org/10.1016/j.scs.2025.106601. July.
Wang, P., Yu, P., Huang, L., & Zhang, Y. (2022). An integrated technical, economic, and environmental framework for evaluating the rooftop photovoltaic potential of old residential buildings. *Journal of Environmental Management, 317*, Article 115296. https://doi.org/10.1016/j.jenvman.2022.115296. Sept.
Wang, P., Yu, P., Huang, L., & Zhang, Y. (2022). An integrated technical, economic, and environmental framework for evaluating the rooftop photovoltaic potential of old residential buildings. *Journal of Environmental Management, 317*, Article 115296. https://doi.org/10.1016/j.jenvman.2022.115296. Sept.
Wei, T., Zhang, Y., Zhang, Y., Miao, R., Kang, J., & Qi, H. (2024). City-scale roof-top photovoltaic deployment planning. *Applied Energy, 368*, Article 123461. https://doi.org/10.1016/j.apenergy.2024.123461. Aug.
Yan, L., et al. (2023). Estimation of urban-scale photovoltaic potential: A deep learning-based approach for constructing three-dimensional building models from optical remote sensing imagery. *Sustainable Cities and Society, 93*, Article 104515. https://doi.org/10.1016/j.scs.2023.104515. June.
Yang, J., Wu, J., Lu, J., Peng, X., Yuan, H., & Lai, L. L. (2024). A novel method for assessment rooftop PV potential based on remote sensing images. *Renewable Energy, 237*, Article 121810. https://doi.org/10.1016/j.renene.2024.121810. Dec.
Yu, Y., Chou, J., Xiao, Y., & Yang, L. (2023). Classification of building complex for the large-scale construction of distributed photovoltaics in urban buildings. *Energy and*

Buildings, 300, Article 113677. https://doi.org/10.1016/j.enbuild.2023.113677. Dec.

Yu, S., Han, R., & Zhang, J. (2023). Reassessment of the potential for centralized and distributed photovoltaic power generation in China: On a prefecture-level city scale. *Energy, 262*, Article 125436. https://doi.org/10.1016/j.energy.2022.125436. Jan.

Yuan, J., Farnham, C., Emura, K., & Lu, S. (2016). A method to estimate the potential of rooftop photovoltaic power generation for a region. *Urban Climate, 17*, 1–19. https://doi.org/10.1016/j.uclim.2016.03.001. Sept.

Zhang, Z., et al. (2023). Carbon mitigation potential afforded by rooftop photovoltaic in China. *Nat Commun, 14*(1), 2347. https://doi.org/10.1038/s41467-023-38079-3. Apr.

Zhang, Y., Han, X., Wei, T., Zhao, X., & Zhang, Y. (2023). Techno-environmental-economical performance of allocating multiple energy storage resources for multi-scale and multi-type urban forms towards low carbon district. *Sustainable Cities and Society, 99*, Article 104974. https://doi.org/10.1016/j.scs.2023.104974. Dec.

Zhang, Y., Han, X., Wei, T., Zhao, X., & Zhang, Y. (2023). Techno-environmental-economical performance of allocating multiple energy storage resources for multi-scale and multi-type urban forms towards low carbon district. *Sustainable Cities and Society, 99*, Article 104974. https://doi.org/10.1016/j.scs.2023.104974. Dec.

Zhao, O., et al. (2022). Investigation of indoor environment and thermal comfort of building installed with bifacial PV modules. *Sustainable Cities and Society, 76*, Article 103463. https://doi.org/10.1016/j.scs.2021.103463. Jan.

Zhu, R., Wong, M. S., Kwan, M.-P., Chen, M., Santi, P., & Ratti, C. (2022). An economically feasible optimization of photovoltaic provision using real electricity demand: A case study in New York city. *Sustainable Cities and Society, 78*, Article 103614. https://doi.org/10.1016/j.scs.2021.103614. Mar.